Microemulsion Polymerization. 3. Molecular Weight and Particle Size Distributions

Carlos C. Co,[†] Patricia Cotts,[‡] Stefan Burauer,[§] Renko de Vries,[†] and Eric W. Kaler*[,†]

Department of Chemical Engineering, University of Delaware, Newark, Delaware 19716; DuPont Central Research and Development, Wilmington, Delaware 19880-0356; and Institut fur Physikalische Chemie, Universität zu Köln, D-50939 Köln, Germany

Received July 18, 2000; Revised Manuscript Received January 2, 2001

ABSTRACT: Molecular weight and particle size distributions of latexes prepared by free radical polymerization of *n*-butyl methacrylate, *tert*-butyl methacrylate, *n*-hexyl methacrylate, and styrene in aqueous microemulsions of dodecyltrimethylammonium bromide surfactant are measured using GPC/MALLS, QLS, and cryo-TEM. The results are compared to a molecular weight distribution model derived from the monomer partitioning and kinetic studies described in the accompanying papers. Polystyrene with weight-average molecular weights of $\sim 15 \times 10^6$ Da, which are 7 times greater than the limiting molecular weight imposed by chain transfer to monomer, are consistently obtained. Diffusion-limited exit of monomer radicals, generated by chain transfer, to the aqueous phase coupled with chain transfer to polymer are likely reasons for the enhanced polystyrene molecular weights.

1. Introduction

In the first two parts of this series, the influence of monomer partitioning, biradical termination, and glass transition on microemulsion polymerization kinetics were investigated. In this third part, the molecular weight and particle size distributions (MWDs and PSDs) of the final latex product are measured and compared to calculations from a MWD model based on the mechanistic description presented in part 2. PSDs measured as part of the equilibrium monomer partitioning SANS studies in part 1 are also confirmed by direct imaging using cryo-TEM and compared with dynamic light scattering (DLS) results.

The current MWD model is an extension of our previous MWD model,[1] now modified to account for biradical termination and nonlinear monomer partitioning. Efforts in directly testing the MWD model have previously been hampered by difficulties in accurately measuring the very high molecular weight ($\sim 15 \times 10^6$ Da) of the microemulsion polymers. A large part of this inaccuracy has now been eliminated through careful chromatographic analysis using recently commercialized nonshedding columns and a multiangle light scattering detector.

Interestingly, we regularly obtain very high molecular weights of $\sim 15 \times 10^6$ Da for styrene microemulsion polymerizations. Such molecular weights are considerably higher than that typically obtained via free-radical polymerizations. Chain transfer to monomer limits styrene free-radical polymerizations to weight-average molecular weights of $\sim 2 \times 10^6$ Da as suggested by the most recent measurements of chain-transfer constants by Kukulj et al.[2] The enhancement in the polystyrene molecular weight in microemulsion polymerizations is likely due to chain transfer to polymer. In a previous paper,[3] we have suggested that long-chain branching complicates the chromatographic analysis. However, the present and more accurate measurements demonstrate that the extent of chain branching is so low that no difference can be detected in the size of the microemulsion polymers and linear standards in solution.

2. Materials and Methods

2.1. Particle Sizing. Samples for cryo-TEM were prepared at room temperature by placing a 5 μL drop of the polymerized microemulsion on a holey carbon film supported on a TEM copper grid. The drop was blotted by filter paper to create a thin film of the liquid over the holes, and the grid was then plunged into liquid ethane slightly above its freezing point at −183 °C. The vitrified sample was mounted in a preparation chamber (Zeiss GA G34-215), filled with liquid nitrogen, and then transferred to a cold stage (Oxford CT 3500). The transmission electron microscope (LEO 912, Leo Elektronenmikroskopie) was equipped with an in-column energy filter and operated at 100 kV. The sample was kept at −175 °C during observation, and using the minimal dose focusing device of the microscope allowed a low dose of 250 electrons/nm^2. Energy-filtered images, with the spectrometer slit aperture set to 15 eV, were recorded with a high-speed scanning camera (1024 × 1024 pixels, Proscan model TH 7896 M) under remote control from an imaging acquisition system (EsiVision AnalySIS 2.11). Several pictures were taken from different positions on each grid, and particle sizing was done using the EsiVision software. In the determination of the size distribution, polymer particles were counted only if their complete circumference is visible. This sample preparation and data analysis procedure was repeated at least twice for each sample to ascertain the reproducibility of the measured PSDs.

The DLS measurements were performed using a cylindrical glass cell (Schott boron silicate glass) filled with 1 mL of sample and sealed with glass stopper. The cells have an internal diameter of 7 mm and an external diameter of 10 mm. The DLS measurements were all performed at a constant temperature of 25 °C on three different instrument setups. The first two instruments are both equipped with ALV-5000C correlators and have Ar ion and He−Ne lasers operating at wavelengths of $\lambda = 488$ nm and $\lambda = 633$ nm, respectively. Measurements were taken at scattering angles from 30° to 150° in 10° increments. A fiber-optic-based DLS instrument

[†] University of Delaware.
[‡] DuPont Central Research and Development.
[§] Universität zu Köln.
* Corresponding author. Tel (302) 831-3553; Fax (302) 831-8201; E-mail kaler@che.udel.edu.

10.1021/ma001248b CCC: $20.00
Published on Web 04/05/2001

(FOQELS) from Brookhaven Instruments equipped with a BIC-9000 correlator operating at a scattering angle of 155° and a wavelength of $\lambda = 671$ nm was also used. The samples were diluted with D_2O until the diameter determined by DLS measurements did not change any more.[4] The analysis of the normalized second-order autocorrelation functions $g^{(2)}(t)$ was done using CONTIN[5,6] to yield intensity distributed diffusion coefficients and corresponding mean hydrodynamic diameters through the Stokes−Einstein relationship. The validity of this analysis depends critically on the absence of multiple scattering and particle interactions. Hence, the samples were sequentially diluted after each measurement until no changes in the measured particle diameters were detected. The accuracy of our cryo-TEM and DLS protocols was tested using three standard latex samples. These standard latexes had diameters of 19 nm (Lot CA94303, Nanosphere, Duke Scientific), 64 nm, and 107 nm (Lot 447000 and Lot 441777, Polybead, Polyscience) as measured using TEM by their respective manufacturers.

The intensity weighted diffusion coefficients measured by DLS result in an average hydrodynamic diameter that is approximately the ratio of the sixth and fifth moments of the PSD (harmonic *z*-average)[1,7]

$$\bar{d}_{\mathrm{DLS}} = \frac{\sum_i n_i d_i^{\,6}}{\sum_i n_i d_i^{\,5}} \tag{1}$$

Hence, for polydisperse samples, the average diameters obtained using DLS would be significantly higher than the number-average diameters measured using cryo-TEM. For comparative purposes, eq 1 can be used to obtain approximate average DLS-weighted diameters from the cryo-TEM results. Note however that the effective number of particles involved in establishing an average DLS diameter is many orders of magnitude larger than the number imaged in any cryo-TEM photograph. Thus, the presence of a small concentration of larger latex or dust particles,[8] which can severely distort the DLS measurements toward larger diameters, may not be accounted for completely by eq 1. Finally, even for a perfectly monodisperse sample, DLS measures a hydrodynamic diameter that is expected to be slightly larger than the true particle size.

2.2. MWD Analysis. MWDs were measured using size exclusion chromatography (SEC) coupled with a multiangle laser light scattering detector (MALLS, Wyatt DAWN DSP) and a differential refractive index (Waters R410) detector. Nonshedding PL-Gel Mixed-A LS columns from Polymer Laboratories with a nominal fractionation range from 2×10^3 to 40×10^6 Da were used. The very high molecular weights and low polydispersities of the microemulsion polymerized samples require high dilutions to minimize column overloading and/or apparent shear degradation. A flow rate of 0.5 mL/min was used, and polymer concentrations as low as 5 ppm were found to be necessary. Reliable determination of the eluting concentration from the differential refractive index increment required the use of stabilized tetrahydrofuran (THF) for the mobile phase, precise above-ambient temperature control (40 °C), and long equilibration times (several hours). Offline static and dynamic light scattering measurements were also performed to confirm the chromatographic results. The data were acquired using a Brookhaven goniometer and BI9000 correlator.

Latex samples for molecular weight analysis were taken from the reactor over the course of the online SANS experiments described in part 2 and precipitated directly into a large excess of methanol. Repeated washings with methanol reduced the concentration of dodecyltrimethylammonium bromide (DTAB) surfactant in the polymer to ~1.5 wt %, as determined by bromine analysis on the combusted polymer samples. This level of surfactant in the polymer has no influence on the chromatographic separation. Indeed, the log M vs elution volume curves of a polystyrene standard (Polymer Standard Service, 23×10^6 Da) with and without 5 wt % of additional DTAB were essentially identical.

Typically, the polymers are all insoluble in methanol. However, given the high relative concentration of surfactant to polymer, adsorbed surfactant may cause some polymer to be solubilized in the methanol solvent. To ensure that polymer is not lost during the methanol precipitation step, some of the original aqueous latex samples were dialyzed (12×10^3 Da cutoff regenerated cellulose membranes) against methanol. No significant differences in the MWDs of the samples prepared by precipitation and dialysis were observed.

3. Theory

The MWDs are calculated using a direct extension of our previous theory[1] now corrected to account for the effects of biradical termination and nonlinear monomer partitioning as discussed in parts 1 and 2. The rate equation for the number of growing chains (N^*) in terms of the rate of initiation ($\bar{\rho}$) and the efficiency of chain stoppage ($\bar{\gamma}$) is given by

$$\frac{\partial N^*}{\partial t} = \bar{\rho}(t) - \bar{\gamma}(t)N^* \tag{2}$$

As discussed in part 2, only a fraction (P_{prop}) of the initiator-derived and transfer-generated radicals are available to initiate new chains. Hence, following the nomenclature introduced in the previous papers, the rate of initiation of new chains is

$$\bar{\rho}(t) = (\rho + k_{\mathrm{tr}} C_{\mathrm{mon}}^{(\mathrm{part})} N^*) P_{\mathrm{prop}} \tag{3}$$

Chain stoppage may be due to chain transfer to monomer or biradical termination. Therefore, the efficiency of chain stoppage is given by

$$\bar{\gamma}(t) = k_{\mathrm{tr}} C_{\mathrm{mon}}^{(\mathrm{part})} + (k_{\mathrm{tr}} C_{\mathrm{mon}}^{(\mathrm{part})} + \rho/N^*) P_{\mathrm{term}} \tag{4}$$

The time dependence of $\bar{\rho}$ and $\bar{\gamma}$ arises since the concentration of monomer in the particles ($C_{\mathrm{mon}}^{(\mathrm{part})}$), as well as P_{prop} and P_{term}, all depend on time.

For chains initiated between time t_1 and $t_1 + \mathrm{d}t$, only a fraction $P_{\mathrm{live}}(t_1,t)$ of these will still be growing at a later time t. Expressed in terms of the efficiency of chain stoppage, the rate equation for $P_{\mathrm{live}}(t_1,t)$ is

$$\frac{\partial P_{\mathrm{live}}(t_1,t)}{\partial t} = -\bar{\gamma}(t) P_{\mathrm{live}}(t_1,t) \tag{5}$$

Likewise, the normalized probability $P_{\mathrm{dead}}(t_1,t)$ that a chain initiated at time t_1 stops growing at a later time t is

$$P_{\mathrm{dead}}(t_1,t) = -\frac{\partial P_{\mathrm{live}}(t_1,t)}{\partial t} = \bar{\gamma}(t) P_{\mathrm{live}}(t_1,t) \tag{6}$$

Integration of eq 5 gives $P_{\mathrm{live}}(t_1,t)$ and $P_{\mathrm{dead}}(t_1,t)$

$$P_{\mathrm{live}}(t_1,t) = \frac{P_{\mathrm{dead}}(t_1,t)}{\bar{\gamma}(t_1,t)} = \exp\left(-\int_{t_1}^{t} \bar{\gamma}(t')\,\mathrm{d}t'\right) \tag{7}$$

Following the derivation of our previous model for the MWD,[1] the kinetic chain length $L(t_1,t)$ of a chain that has grown from t_1 to t is

$$L(t_1,t) = \int_{t_1}^{t} k_{\mathrm{p}} C_{\mathrm{mon}}^{(\mathrm{part})}(t')\,\mathrm{d}t' \tag{8}$$

Taking the inverse of this expression gives the earlier time $t_1(L,t)$ at which a chain must have been initiated to grow to a length L at time t. Note that the inverse does not exist for times $t < t_{min}(L)$ that are too short to allow the growth of a polymer chain consisting of L monomer units.

The number density $n(L,t)$ of chains with L monomer units at time t has contributions from both live and dead polymer chains

$$n(L,t) = n_{live}(L,t) + n_{dead}(L,t) \tag{9}$$

Live chains that have grown to a length L at time t must have been initiated during a small interval of time around $t_1(L,t)$. The duration $\tau(L,t)$ of this interval is the inverse of the propagation rate at time $t_1(L,t)$, i.e., the time interval for one propagation event.

$$\tau(L,t) = \frac{1}{k_p C_{mon}^{(part)}(t_1(L,t))} \tag{10}$$

The total number of chains initiated in this interval is then simply $\tau(L,t)\,\bar{\rho}(t_1(L,t))$. Of these, a fraction $P_{live}(t_1,t)$ are still growing at time t. Therefore, the contribution of the growing chains to $n(L,t)$ is

$$n_{live}(L,t) = \tau(L,t_1(L,t))\bar{\rho}(t_1(L,t))P_{live}(t_1(L,t),t) \tag{11}$$

Likewise, the contribution of the dead chains is

$$n_{dead}(L,t) = \int_{t_{min}(L)}^{t} \bar{\rho}(t')P_{dead}(t_1(L,t'),t')\,dt' \tag{12}$$

Measured MWDs are typically presented as dw/d(log M) vs log M and normalized such that the total area under the distribution is unity. Here, $w(M)$ is the cumulative MWD and is related to the weight $W(M)$ and number $N(M)$ MWD via

$$W(M) = MN(M) = \frac{dw}{dM} = \frac{\log e}{M}\frac{dw}{d(\log M)} \tag{13}$$

As $W(M)$ is also normalized, the calculated number density $n(L)$ of chains consisting of L monomer units (each monomer unit has molecular weight m) can be compared to the experimental results through

$$W(M) = \frac{Mn\left(\frac{M}{m}\right)}{\int_0^\infty M'n\left(\frac{M'}{m}\right)dM'} \tag{14}$$

$$\frac{n\left(\frac{M}{m}\right)}{\int_0^\infty M'n\left(\frac{M'}{m}\right)dM'} = \frac{\log e}{M^2}\frac{dw}{d(\log M)} \tag{15}$$

In conventional SEC analysis, this relationship is correct only in the region where log M varies linearly with elution volume.[9] However, in our measurements, molecular weights were measured directly using a light scattering detector. Therefore, no assumptions were made regarding the elution characteristics of the polymers even though we plot our measured and calculated results as dw/d(log M) vs log M.

4. Results and Discussion

4.1. Particle Size Distributions. Cryo-TEM imaging was performed on the polymerized microemulsions used for the equilibrium SANS studies described in part 1. A typical image of the polymerized samples (nC_4MA) is shown in Figure 1. A direct comparison of the PSDs obtained using these two techniques is shown in Figure 2. With the possible exception of the tC4MA sample, the agreement between the PSDs measured using the two techniques is well within experimental error and further corroborates the experimental and data analysis protocols.

However, as Table 1 shows, the diameters measured using DLS are almost 2 times larger than the number-

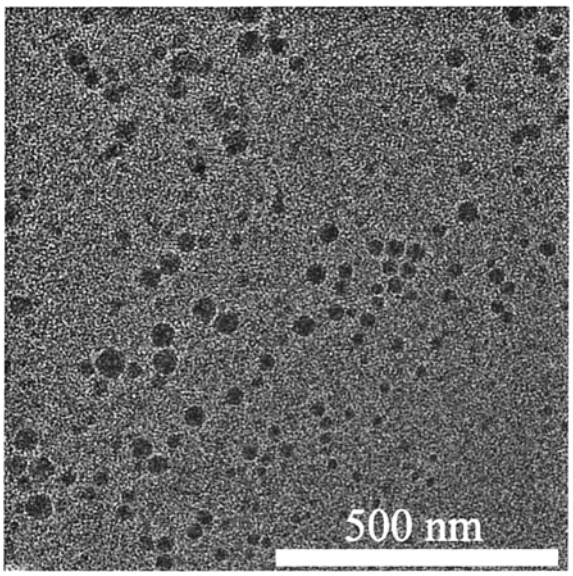

Figure 1. A typical cryo-TEM image of polymerized nC_4MA/DTAB/D_2O microemulsions. The spherical particles and surrounding aqueous solution have very similar electron densities, resulting in weak image contrast.

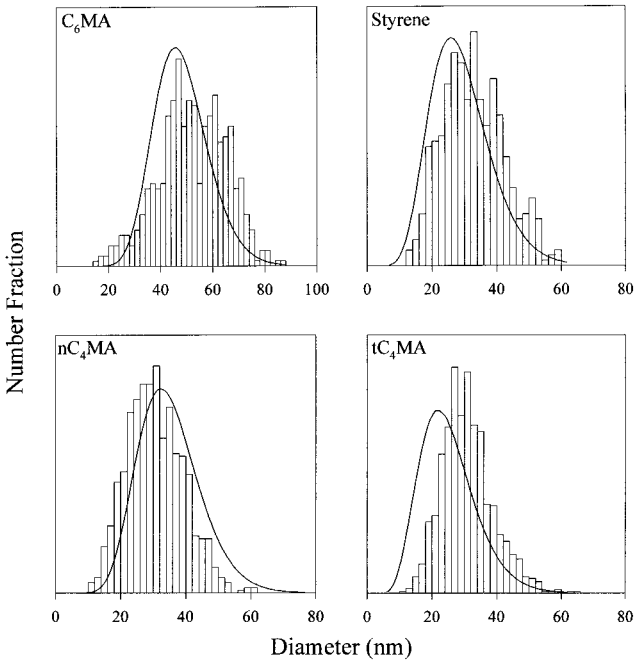

Figure 2. Comparison of the number size distribution as determined by cryo-TEM and SANS for the fully polymerized microemulsion samples used to prepared the samples for equilibrium SANS analysis (part 1). The original microemulsions contained 12 wt % of DTAB surfactant and 3 wt % of monomer on a surfactant-free basis in D_2O. A V50 concentration of 0.063 wt % with respect to monomer was used to initiate the polymerizations at 60 °C.

Table 1. Particle Size Distribution Results from SANS, Cryo-TEM, and DLS

	number avg diameter (nm)					intensity ($\langle d^6\rangle/\langle d^5\rangle$) avg diameter (nm)			
	SANS		cryo-TEM			DLS			cryo-TEM
	avg	std dev	avg	std dev	#	488 nm	633 nm	671 nm	DLS avg
std 19 nm			19	3	187	20	20	19	23
std 64 nm			56	7	169	64	65	64	62
std 107 nm			94	12	338	107	108	108	92
C_6MA	46	10	52	13	539	63	67	64	66
nC_4MA	35	10	31	9	913	57	56	58	42
tC_4MA	25	9	33	9	1158	50	46	45	42
styrene	29	9	33	10	489	50	51	63	45

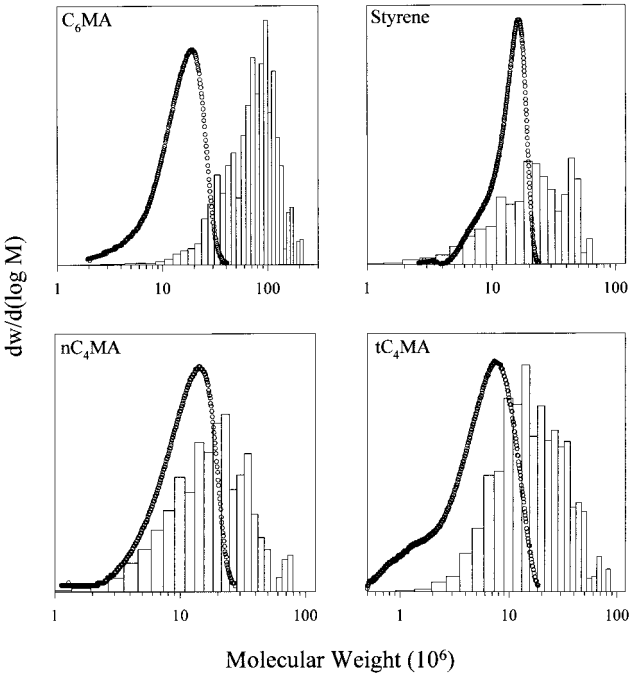

Figure 3. Comparison of the MWDs measured using SEC/MALLS/RI for the polymer samples described in Figure 2 and the corresponding MWDs calculated from the cryo-TEM size distributions presented in Figure 2.

average diameters measured using SANS or cryo-TEM.[8,10] As discussed in section 2, a part of this discrepancy is due to the different weighting used to obtain the averages. Using eq 1 to convert the number-weighted diameter obtained by cryo-TEM shown in Figure 2 to an intensity-weighted diameter gives better agreement. Nevertheless, dimensions measured by DLS are still up to 50% larger than those from cryo-TEM for the microemulsion polymerized latexes. This discrepancy is most likely due to the strong bias of the DLS measurement toward larger particles that may not be fully accounted for by eq 1 due to the finite number of particles measured using cryo-TEM.[8,10,11]

In Figure 3, the corresponding MWDs from the cryo-TEM PSDs, calculated assuming single chain particles, are shown together with the MWDs measured by chromatography and light scattering. With the exception of C_6MA, the positions of the peak in the MWDs obtained from either technique match to within less than a factor of 2. This indicates that a large majority of the particles in the final latex consist of only one or two polymer chains.

The time scale for propagation ($\sim 10^{-3}$ s) is indeed sufficiently long for a small free radical species to enter and exit $\sim 10^3$ micelles before initiating a new polymer chain. This number of entry and exit events is comparable to the number ratio of micelles to particles[3,12] of $\sim 10^3$ and explains why biradical termination cannot always be neglected. However, as Figure 3 indicates, nonnegligible biradical termination occurring via this mechanism does not necessarily lead to multichain particles.

Biradical termination is a fast process that occurs essentially every time a radical enters a particle containing an existing growing radical chain. However, to a first approximation, a radical is about equally likely to propagate upon entering either a micelle or dead polymer particle. Therefore, in contrast to termination, the probabilities of initiating a micelle to form a new particle or initiating a second chain within an existing dead particle is largely independent of the number of entry and exit events the small free radical species undertake prior to propagating. Instead, these probabilities are determined mainly by the large relative difference (10^3) in the number densities of micelles to polymer particles. Hence, small aqueous phase radicals that do not terminate almost always initiate micelles to form new particles and rarely initiate polymerization within dead particles.

On the basis of this analysis, one would have expected even better agreement between the chromatographically measured and cryo-TEM derived MWDs. Some of this discrepancy is possibly due to particle coagulation since the cryo-TEM measurements were completed over a period of many months. It is true that the interdiffusive motion of polymer chains from two glassy polymer particles is very slow. Therefore, upon direct contact, these particles probably form doublets that break apart before irreversible coagulation occurs via interdiffusion of the polymer chains. However, this is not necessarily the case for particles consisting of low-T_g polymer such as C_6MA ($T_g \sim -5$ °C). The larger discrepancy between the MWDs of C_6MA as measured using the two techniques hints that poly-C_6MA latexes are indeed more prone to coagulation than the other three latexes. Note, however, that even after a year of storage at room temperature, the poly-C_6MA latex exhibits no visible indications of particle coagulation.

4.2. MWDs: Measurements and Model Calculations. Figure 4 shows the molecular weight distributions at varying conversions for the C_6MA, nC_4MA, tC_4MA, and styrene microemulsions used during the acquisition of the online SANS spectra described in part 1. The solid curves in these graphs correspond to the model calculations described in section 3 for the MWDs. A summary of the average molecular weights and polydispersities is given in Table 2. The molecular weights of microemulsion polymers are clearly very high ($>10^7$ Da) and remain essentially constant over the course of the reaction. This is consistent with the model assumption that chain stoppage occurs only through

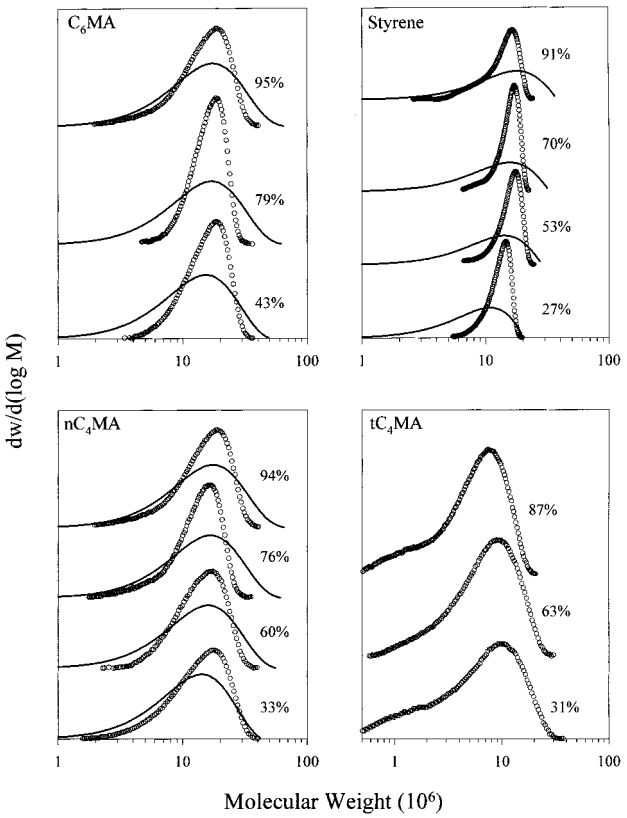

Figure 4. Variation of the MWDs with conversion for microemulsion polymerizations associated with the online SANS experiments described in part 1.

Table 2. Measured and Model Calculated Molecular Weight Averages for Figure 4

		GPC/MALLS/RI		model	
	% conv	M_w (10^6)	M_w/M_n	M_w (10^6)	M_w/M_n
C6MA	95	16	1.3	16	1.8
	79	16	1.1	16	1.8
	43	16	1.2	14	1.8
nC4MA	94	16	1.3	16	1.8
	76	14	1.3	16	1.8
	60	15	1.2	15	1.8
	33	15	1.3	13	1.8
tC4MA	87	6.2	1.8		
	63	8.2	1.6		
	31	7.9	2.4		
styrene	91	14	1.1	15	1.8
	70	15	1.0	14	1.8
	53	16	1.1	13	1.7
	27	13	1.0	9.3	1.6

radical transfer to monomer and, to a much smaller extent, biradical termination.

The model calculations for the MWDs were performed with essentially the same values for all the parameters used in the kinetic model calculations presented in part 2. However, slightly smaller values for the monomer chain-transfer constant (k_{tr}) of 0.015 and 0.013 M^{-1} s^{-1} were used respectively for the C_6MA and nC_4MA MWD calculations to obtain better agreement between the calculated and measured average molecular weights. Note that these values for k_{tr} are well within the range of experimental values (0.007−0.025 M^{-1} s^{-1}) tabulated for the various methacrylates[13] from which we have previously taken a value of 0.02 M^{-1} s^{-1} for the kinetic model calculations presented in part 2. As explained in the following section, the enhanced polystyrene molecular weights are possibly due to a reduction in chain-transfer efficiency caused by glass transition. For tC_4MA microemulsion polymerizations, which also pass through a glass transition, chain transfer to surfactant complicates matters further, and the theory provides no reliable estimate for the molecular weight distribution.

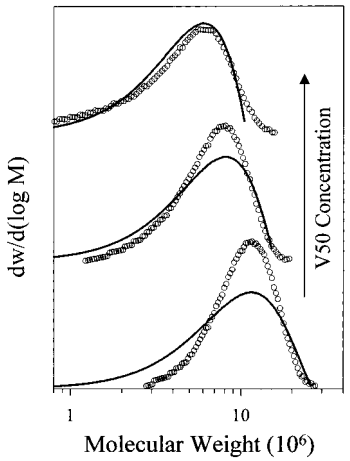

Figure 5. MWDs of fully polymerized C_6MA microemulsions initiated with 1%, 4%, and 10% V50 with respect to monomer at 60 °C. Original microemulsions 12 wt % of DTAB surfactant and 3 wt % of C_6MA on a surfactant-free basis in H_2O.

Table 3. Measured and Model Calculated Molecular Weight Averages for Figure 5

	GPC/MALLS/RI		model	
V50	M_w (10^6)	M_w/M_n	M_w (10^6)	M_w/M_n
1%	11	1.2	10	1.7
4%	7.2	1.2	6.6	1.6
10%	5.0	1.7	4.8	1.5

Surprisingly the measured molecular weight distributions of these polymers are remarkably narrow (M_w/M_n < 1.5) which would seem impossible given the free-radical nature of microemulsion polymerization process. This is borne out by the significantly higher polydispersities ($M_w/M_n \sim 1.8$) that the model described in section 3 predicts. This discrepancy may possibly be due to chromatographic difficulties in fractionating such high molecular weight polymers. Increasing the initiator concentration reduces the molecular weights. This should facilitate chromatographic separation and lead to more accurate polydispersity measurements. Figure 5 shows the MWD of the fully polymerized C_6MA microemulsions initiated with V50 concentration up to 10 wt % relative to monomer. Note that this is 160 times higher than the V50 concentration used to initiate the four previous microemulsion systems. Even at such high initiator concentrations, the experimental and model results, as summarized in Table 3, still do not convincingly show that the low measured polydispersities are merely due to chromatographic limitations.

The model calculations, shown as solid curves in Figure 5, were performed with the same set of parameters used in Figure 4. However, at such high initiator concentrations, aqueous phase termination is expected to reduce the initiator efficiency as described in part 2. To achieve agreement between the model and experimental MWDs, the initiator efficiencies were set at 50%, 35%, and 30% respectively for the systems initiated with 1 wt %, 4 wt %, and 10 wt % V50.

4.3. MWDs: Exceeding the Kinetic Chain Length Limitation. For the microemulsion polymerized styrene samples, the kinetic chain length defined by the

ratio of the propagation[14,15] ($k_p \approx 342$ M^{-1} s^{-1}) and monomer chain-transfer constants[13] ($k_{tr} \approx 0.02$ M^{-1} s^{-1}) of 1.6×10^4 sets a characteristic "limiting" molecular weight of only $\sim 1.6 \times 10^6$ Da for polystyrene. However, the molecular weights of the microemulsion polymerized polystyrene are approximately 10 times higher than this characteristic molecular weight. Consequently, to achieve agreement between the measured and model MWDs, it is necessary to assume a much lower value of 0.002 M^{-1} s^{-1} for the monomer chain-transfer constant of styrene. Indeed, the characteristic molecular weight may be even lower if chain transfer to surfactant is also considered as discussed later. This raises some questions regarding the accuracy of the molecular weight measurements and the nature of the polystyrene formed.

The first concern was whether lower molecular components had been lost during the multiple methanol washings done to remove DTAB surfactant from the polymer. As discussed in section 2, the original polystyrene latexes were dialyzed against methanol using 12 000 molecular weight cutoff regenerated cellulose membranes, and no significant changes in the MWDs were observed. Furthermore, molecular weights and hydrodynamic radii as measured by static and dynamic light scattering experiments were performed on unfractionated polystyrene/THF solutions, and the results were consistent with the SEC/MALLS/RI measurements. Thus, there is no doubt that the weight-average molecular weights of the polystyrene samples are indeed $\sim 15 \times 10^6$ Da—10 times higher than the characteristic molecular weight calculated from literature values for k_{tr}/k_p.

Offline static and dynamic light scattering measurements were also performed on THF solutions of the 91% conversion polystyrene sample. The refractive index increment was $dn/dc = 0.185$ at 488 nm. These samples were neither filtered nor fractionated, and the light scattering measurements were performed using a separate Brookhaven instrument. Inconsistent online and offline measurements would highlight any inaccuracies and artifacts possibly introduced by the chromatographic separation or the light scattering measurements.

The offline static light scattering measurements, presented as a Zimm plot in Figure 6, gives a weight-average molecular weight of $M_w = 13 \times 10^6$ Da and an average radius of gyration of $R_g = 235$ nm that are consistent with the chromatographic measurements. This molecular weight and radius are consistent with other published experimental data for ultrahigh molecular weight polystyrene.[16] Confirming the high molecular weight of these microemulsion polystyrenes via dynamic light scattering is complicated by the angular dependence of the apparent hydrodynamic diameter (d_{app}) measured by QLS (Figure 7). The angular dependence of the apparent diffusion coefficient, which goes as $1/d_{app}$, arises due to the internal motions of the polymer chains and scales with q^2. To obtain the average hydrodynamic diameter (d_h) of entire polymer chains from QLS measurements, the average diffusion coefficient ($\sim 1/d_h$) for center-of-mass translation over long length scales must be obtained by extrapolation to zero angle. The ratio of R_g to $d_h/2$ ranges from 1.5 to 2.0 depending on polydispersity and solvent quality.[17] Figure 7 shows the results of QLS measurements for the 91% conversion polystyrene sample in THF. The average hydrodynamic diameter of the polystyrene ($d_h \approx 260$ nm) is consistent with other published results on polystyrene in THF.[18]

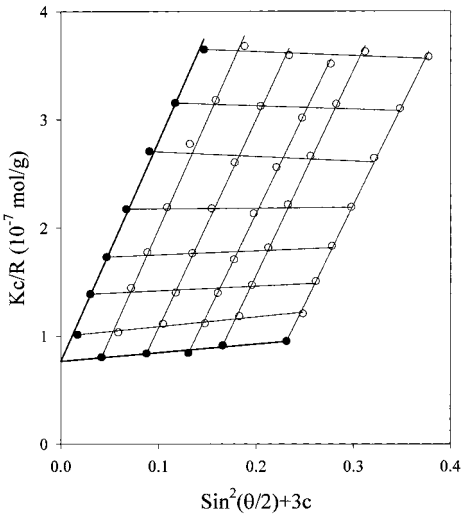

Figure 6. Zimm plot for the 91% conversion polystyrene sample. Light scattering measurements were performed at angles ranging from 15° to 45° in 5° increments on unfiltered THF solutions containing 1.39×10^{-5}, 2.92×10^{-5}, 4.35×10^{-5}, 5.52×10^{-5}, and 7.70×10^{-5} g/cm^3 of polystyrene. Data analysis gives the weight-average molecular weight $M_w = 13 \times 10^6$ Da and the radius of gyration $R_g = 235$ nm.

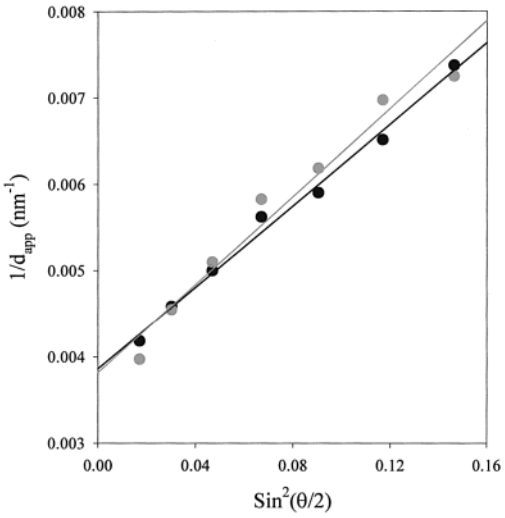

Figure 7. Angular dependence of the apparent hydrodynamic diameter of the 91% conversion polystyrene sample in THF. Data were collected at polymer concentrations of 4.35×10^{-5} (black) and 7.70×10^{-5} g/cm^3 (gray). Extrapolation to zero angle gives the hydrodynamic diameter for center-of-mass translation: $d_h = 259$ nm (black) and 262 nm (gray).

The experimental values for k_{tr} do have some scatter, but the values span a factor of only about 3.[13] Moreover, the value of 0.02 M^{-1} s^{-1} quoted previously is consistent with recent and more accurate measurements of k_{tr} in bulk and emulsion styrene polymerizations.[2,9,19−21] An outlying value of 0.002 M^{-1} s^{-1} that appears to be consistent with our molecular weight measurements has been reported by Pryor and Coco[22] based on computer simulations. However, given the very approximate nature of the simulation, this value is likely unreliable.

Given the chemical nature of the propagation and monomer chain-transfer processes, one would expect the ratio k_{tr}/k_p to be essentially the same for bulk, emulsion, and microemulsion polymerizations as the chemical environment of the reacting site are the same. It has

been suggested that the chain-transfer mechanism for styrene may involve hydrogen abstraction from the Diels−Alder dimer,[23,24] the concentration of which may depend on the polymerization conditions. However, experimental measurements of k_{tr}/k_p have yielded the same values for both bulk and emulsion polymerizations,[2,9,21] and there is no reason to expect otherwise for the present styrene microemulsion system.

Thus, there must be another explanation for the high molecular weight observed, and a logical candidate is that diffusion limitations reduce the effectiveness of chain transfer to monomer. The monomer partitioning and kinetic studies reported in parts 1 and 2 indicate the possibility of glass transition effects setting in even at low conversions (<30%). If this is true, then for the present styrene microemulsion, a large proportion of the polymerization reaction occurs under diffusion-limited conditions. However, diffusion-limited transport of monomer to the reacting site alone will clearly not alter the ratio k_{tr}/k_p and hence the limiting molecular weight as Casey et al.[25] have noted. Instead, to have a chance of exceeding the limiting molecular weight imposed by k_{tr}/k_p, diffusion of the transfer-generated monomeric radical must be limited such that it propagates within the same particle and through chain transfer to polymer, eventually linked back to the original polymer.

As shown in ref 9, the diffusion coefficient of styrene drops to 10^{-12} m^2 s^{-1} as the volume fraction of monomer in the polystyrene particles decreases to 20 vol %. For this value of the diffusion coefficient, the time scale for diffusion across the ∼30 nm glassy particles is on the order of 10^{-3} s, which is also the time required for a typical propagation event (as calculated in part 2). Note that such low monomer volume fractions in the particles are reached early on in the reaction (∼40% conversion) as measured in part 1. Therefore, a styrene radical generated by chain transfer has a high probability of propagating within the same particle.

Under conditions where propagation is limited by monomer diffusion, the movement of the radical chain end via reaction−diffusion[26] becomes important. In the extreme case where steep monomer concentration gradients are present and the chain end can move only by reacting with monomer, the average movement of the radical end becomes directed toward the steepest concentration gradient. Hence, the reaction will occur mainly at the interface. In the other limit where the random diffusive motion of the chain end dominates, concentration gradients disappear, and there is an equal probability of finding the chain end in any differential volume throughout the particle. However, even in this situation, the probability of finding the radical end at a distance $r + \delta r$ from the center of a particle still scales as r^2 due to the spherical geometry. Since the interface of the particles is most likely fully covered with surfactant, chain transfer to the surfactant hydrocarbon tail via hydrogen abstraction can be significant. Although the chain-transfer constants to the DTAB surfactant have not been measured, they should be comparable to the chain-transfer constants to unsubstituted hydrocarbon solvents. For methyl methacrylate and styrene the chain-transfer constants to heptane are ∼18 and ∼0.7 times their respective monomer chain-transfer constants.[13] Therefore, chain transfer to surfactant may have a significant influence on the MWD of the methacrylates. This is particularly true for tC_4MA microemulsion polymerizations where the polymer particles become glassy at low conversions (part 2), and the radical end may be directed toward the interface via reaction−diffusion.

Transfer-generated monomeric radicals typically exit and initiate the growth of new particles unless the diffusion coefficient is reduced significantly by glass transition as described previously. Transfer-generated surfactant radicals, that are not resonance stabilized, are expected to be $\sim 10^3$ times more reactive than a styrene radical.[27] Thus, the surfactant radical propagates within $\sim 10^{-6}$ s, which is comparable to the typical surfactant residence times of $10^{-6}-10^{-5}$ s. Hence, during styrene microemulsion polymerizations, a transfer-generated surfactant radical tends to initiate a new chain within the same particle. However, this is clearly not the case during the microemulsion polymerization of *tert*-butyl methacrylate that has the lowest molecular weight among the four microemulsion polymers shown in Figure 4 and Table 2.

Because of their lack of resonance stabilization, acrylonitrile, methyl acrylate, and vinyl acetate are all much less reactive than styrene toward radicals.[27] However, tabulated copolymerization reactivity ratios[13] for typical substituted monomers cannot be explained solely on resonance effects, and the relative polarity of substituents must be also taken into account. Nevertheless, for aliphatic radicals with nonpolar substituents, resonance effects are expected to be dominant, and we hypothesize that methacrylates are significantly less reactive in comparison to styrene toward surfactant radicals. If this is true, then transfer-generated surfactant radicals propagate more slowly in methacrylate microemulsions and thus have a greater tendency to exit and initiate new particles as compared to their counterparts in styrene microemulsions. This difference is particularly important for tC_4MA microemulsion polymerizations for which chain transfer to surfactant is also expected to occur most frequently. Repropagation of transfer-generated radicals within their parent particles is critical in exceeding the molecular weight limitations imposed by chain transfer. Unlike styrene, chain transfer to surfactant limits the maximum molecular weight that can be obtained from tC_4MA microemulsion polymerizations.

Chain transfer to either monomer or surfactant followed by initiation of a new chain within the same particle alone will not increase the polystyrene molecular weights beyond the limiting molecular weight imposed by the ratio k_{tr}/k_p. In addition, at least two polymer chain-transfer events must take place to link the new and old polymer chains. Accurate measurement of chain transfer to polymer is very difficult as it involves measuring the average number of branch points per chain. However, since chain transfer to polymer and monomer both typically occur via hydrogen abstraction, one would expect these rate constants to be similar for a given monomer. This is indeed true for many monomers including methyl methacrylate and styrene. Given that the locus of polymerization in present styrene microemulsion system is typically more concentrated in polymer segments than monomer (part 2), chain transfer to polymer can be expected to occur at a frequency at least equal to chain transfer to monomer. In either case, however, chain-transfer events are rare, occurring on average only once every $\sim 10^5$ propagation events.

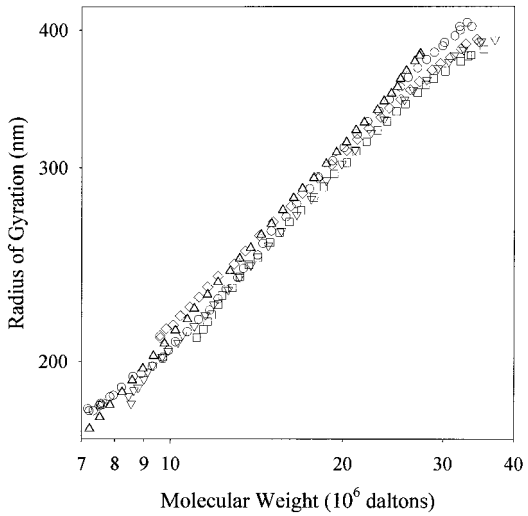

Figure 8. Variation of R_g with MW associated with the polystyrene MWDs presented in Figure 4 (○, 27%; □, 53%; ◇, 70%; ▽, 91%) and (▲) for a linear polystyrene standard from Polymer Standard Service with nominal MW of 23 × 10^6 Da.

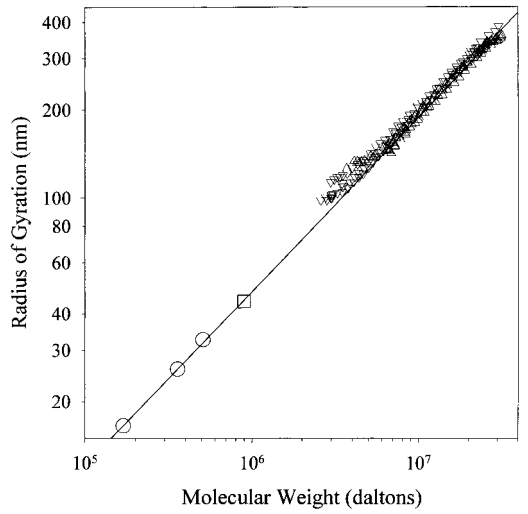

Figure 9. Variation of R_g with MW associated with the (△) nC_4MA and (▼) tC_4MA MWDs presented in Figure 4 and for linear (○) nC_4MA and (□) tC_4MA standards from Polymer Standard Service.

4.3. MWDs: Size, Polydispersity, and Elution Profiles. Extensive chain transfer to polymer results in branching that reduces the radius of gyration (R_g) for polymers of a given molecular weight. Figure 8 shows a comparison of the variation of R_g with MW for a linear polystyrene standard (Polymer Standard Service, 23 × 10^6 Da) and for the microemulsion polymerized styrene samples taken at varying conversions that correspond to the MWDs presented in Figure 4. The excellent agreement between the standard and microemulsion polymerized styrene samples clearly indicates that chain transfer to polymer is minimal and undetectable. An equally good agreement is observed between the R_g vs MW curves for linear standards and microemulsion polymerized butyl methacrylates as shown in Figure 9. More sensitive rheological measurements might provide some estimate of the extent of chain branching.

As mentioned previously, the extraordinarily low polydispersities reported in Table 2 and Figure 4 are very surprising given the free-radical nature of the microemulsion polymerization process. Indeed, the MWD model presented in section 3, which assumes that chain stoppage occurs only by termination or chain transfer and ignores other possible MWD broadening mechanisms, still predicts distributions with polydispersities of ∼1.8 that are broader than those observed. As mentioned in section 2, it is necessary to use very low polymer concentrations to avoid column overloading. Since the light scattering signal scales with the square of the molecular weight, the MALLS detector may not have adequate dynamic range to detect the high (>15 × 10^6) and low molecular weight components simultaneously. However, this explanation is not entirely consistent with the noticeably higher polydispersities measured for the microemulsion poly-tC_4MA (Figure 4 and Table 2) and the low polydispersities measured even for the microemulsion poly-C_6MA initiated with very high V50 concentrations (Figure 5 and Table 3). Nevertheless, in the absence of overwhelming evidence to support the monodispersity of the microemulsion polymers, we cannot rule out the possibility that the low measured polydispersities reflect instrumental limitations. However, the even lower measured polydispersities of the microemulsion polymerized styrene samples beg further discussion.

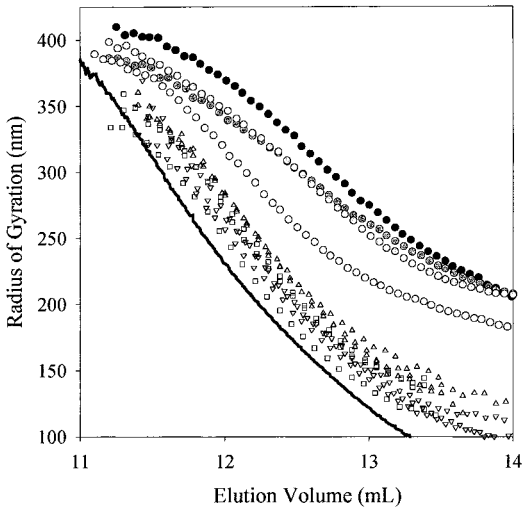

Figure 10. Variation of R_g with elution volume associated with the (□) C_6MA, (△) nC_4MA, (▽) tC_4MA, and (○) styrene MWDs presented in Figure 4. With increasing shading intensity, the circular symbols correspond respectively to the polystyrene samples taken at (○) 27%, (◑) 53%, (●) 70%, and (●) 91% conversion. The solid elution curve is for a linear polystyrene standard from Polymer Standard Service with nominal MW of 23 × 10^6 Da.

Figure 10 shows the variation of R_g with elution volume during the measurement of the MWDs presented in Figure 4. All three methacrylates have elution profiles that are similar to that of the linear polystyrene standard. Interestingly, the discrepancy between the elution profile for the microemulsion polymerized styrene and the linear polystyrene standard increases with conversion. Very clearly, size exclusion is not the only mode of separation for the microemulsion polystyrene. An additional attractive interaction exists between the microemulsion polystyrenes and the chromatographic packing.

Initially, residual DTAB surfactant (∼1.5 wt % via bromine analysis) in the microemulsion polystyrene was suspected to be the cause of this discrepancy. However, addition of ∼5 wt % of DTAB to the polystyrene standard caused no changes in its elution characteris-

tics. Nevertheless, there is no component in the styrene microemulsion systems other than the surfactant that is present at concentrations sufficient to significantly alter the elution characteristics of the polystyrene product. Although adsorbed surfactant has been shown to have no effect, transfer-generated surfactant covalently bound to the microemulsion polystyrene may cause the abnormal elution profiles. Chain transfer to surfactant becomes increasingly frequent as the monomer is used up. Therefore, this mechanism would also explain the increasing discrepancy in the elution profiles with increasing conversion. Accurately measuring the low concentration of covalently bound surfactant is complicated by the presence of residual adsorbed surfactant. At this point, there is no thoroughly convincing evidence for the presence of surfactant covalently bound to microemulsion polymerized styrene.

Anomalous elution behavior has been reported recently in the literature for several different very high molecular weight polymers.[28−30] In most cases, delayed elution is observed for some of the polymer and has been attributed to "sieving" or entrapment. At exceptionally high molecular weight, as the end-to-end distance of the polymer molecules approaches a size comparable to the interstitial voids between the spheres of the column packing, the chains may be forced to reptate, leading to delayed elution. The effect is most often observed with branched polymers of exceptionally high molecular weight.

4.4. Kinetic Consequences of Reduced Chain-Transfer Efficiency. A reduction in chain-transfer efficiency is the only possible explanation for the ultrahigh polystyrene molecular weights. Regardless of whether this diminished efficiency is indeed caused by diffusion limitations, the effective value of the chain transfer constant has been decreased by an order of magnitude to $\sim$0.002 M^{-1} s^{-1}. Observe in Table 2 that very high MW polystyrene (13×10^6 Da) is already obtained, and hence, chain-transfer efficiencies have already been diminished even at 27% conversion. The accompanying reduction in the rate of production of transfer generated radicals is expected to affect the kinetics through a commensurate reduction in the rate of biradical termination.

If we insist that diffusion limitations are absent as initially assumed in part 2, the same kinetic model can be used to calculate polymerization rates. Not surprisingly, substitution of this reduced value for k_{tr} into the kinetic model requires that the characteristic time scale for termination (τ_{term}) be decreased significantly from 1.9×10^{-6} to 0.4×10^{-6} s to achieve agreement with the experimental kinetics. As discussed in part 2, τ_{term} values for nC_4MA and styrene microemulsion polymerizations are expected to be similar. Yet, using this reduced value of $\tau_{term} = 0.4 \times 10^6$ s in calculating the nC_4MA kinetics would drastically underpredict the rate of polymerizations and also shift the maximum rate of polymerizations to $\sim$20% conversion. This contradiction, albeit requiring some assumptions, supports the idea that diffusion limitations indeed play an important role during styrene microemulsion polymerizations even at low conversions (<30%).

5. Conclusions

Particle sizing via SANS and cryo-TEM confirms that microemulsion polymerization systems permit the facile preparation of small latex particles with diameters of about 30 nm. The *z*-average particle diameters measured by DLS are biased toward larger particles and hence are up to 2 times larger than that measured by SANS and cryo-TEM. Comparison of the polymer MWDs with the corresponding MWDs of the particles indicates that the particles contain on average only one or two chains.

For C_6MA and nC_4MA, the MWD model accurately predicts the average polymer molecular weights with parameter values consistent with independent measurements. However, the extraordinarily high molecular weights measured for polystyrene require a value for the chain-transfer constant to monomer that is 10 times less than literature values. It is proposed that this enhancement in the average molecular weight is due to a combination of diffusion limitations and chain transfer to polymer. Chain transfer to surfactant is suspected to play a more important role for tC_4MA compared to styrene microemulsion polymerizations. A potential enhancement in the molecular weights of microemulsion poly-tC_4MA due to diffusion limitations and chain transfer to polymer is not observed possibly due to limitations imposed by chain transfer to surfactant. In all cases, however, the measured polydispersities (M_w/M_n) are considerably smaller than the theoretical predictions, and this is likely the result of analytical challenges in measuring the MWDs of such high molecular weight polymers.

Acknowledgment. S. Burauer thanks Prof. R. Strey and Dr. L. Belkoura (both Universität zu Köln) for help and discussions on DLS and cryo-TEM size distributions. We also thank Joseph Galperin and Peggy Foster for technical assistance with the SEC/MALLS and off-line static and dynamic light scattering.

References and Notes

(1) Morgan, J. D.; Kaler, E. W. *Macromolecules* **1998**, *31*, 3197.
(2) Kukulj, D.; Davis, T. P.; Gilbert, R. G. *Macromolecules* **1998**, *31*, 994.
(3) Co, C. C.; Kaler, E. W. *Macromolecules* **1998**, *31*, 3203.
(4) Burauer, S.; Belkoura, L.; Strey, R.; Co, C.; Kaler, E. *Elektronemikroskopie*, submitted.
(5) Provencher, S. W. *Comput. Phys. Commun.* **1982**, *27*, 213.
(6) Provencher, S. W. *Comput. Phys. Commun.* **1982**, *27*, 229.
(7) Finsy, R.; De Jaeger, N. *Part. Part. Syst. Charact.* **1991**, *8*, 187.
(8) Egelhaaf, S. U.; Wehlri, E.; Muller, M.; Adrian, M.; Shurtenberger, P. *J. Microsc.* **1996**, *184*, 214.
(9) Gilbert, R. G. *Emulsion Polymerization: A Mechanistic Approach*; Academic Press: San Diego, 1995.
(10) De Smet, Y.; Danino, D.; Deriemaker, L.; Talmon, Y.; Finsy, R. *Langmuir* **2000**, *16*, 961.
(11) Talmon, Y. *Ber. Bunsen-Ges. Phys. Chem.* **1996**, *100*, 364.
(12) Full, A. P.; Kaler, E. W.; Arellano, J.; Puig, J. E. *Macromolecules* **1996**, *29*, 2764.
(13) *Polymer Handbook*, 3rd ed.; Brandrup, J., Immergut, E. H., Eds.; John Wiley & Sons: New York, 1989.
(14) Deady, M.; Mau, A. W. H.; Moad, G.; Spurling, T. H. *Makromol. Chem.* **1993**, *194*, 1691.
(15) Hutchinson, R. A.; Aronson, M. T.; Richards, J. R. *Macromolecules* **1993**, *26*, 6410.
(16) Appelt, B.; Meyerhoff, G. *Macromolecules* **1980**, *13*, 657.
(17) Burchard, W. *Adv. Polym. Sci.* **1999**, *143*, 113.
(18) Duval, M.; Lutz, P.; Strazielle, C. *Makromol. Chem., Rapid Commun.* **1985**, *6*, 71.
(19) Whang, B. C. Y.; Ballard, M. J.; Napper, D. H.; Gilbert, R. G. *Aust. J. Chem.* **1991**, *44*, 1133.
(20) Clay, P. A.; Gilbert, R. G.; Russell, G. T. *Macromolecules* **1997**, *30*, 1935.
(21) Miller, C. M.; Clay, P. A.; Gilbert, R. G.; El-Aasser, M. S. *J. Polym. Sci., Polym. Chem.* **1997**, *35*, 989.

(22) Pryor, W. A.; Coco, J. H. *Macromolecules* **1970**, *3*, 500.
(23) Olah, O. F.; Kauffmann, H. F.; Breitenbach, J. W. *Makromol. Chem.* **1976**, *177*, 3065.
(24) Olah, O. F.; Kauffmann, H. F.; Breitenbach, J. W. *Makromol. Chem.* **1977**, *178*, 2707.
(25) Casey, B. S.; Mills, M. F.; Sangster, D. F.; Gilbert, R. G.; Napper, D. H. *Macromolecules* **1992**, *25*, 7063.
(26) Russell, G. T.; Napper, D. H.; Gilbert, R. G. *Macromolecules* **1988**, *21*, 2133.
(27) Hiemenz, P. C. *Polymer Chemistry: The Basic Concepts*; M. Dekker: New York, 1984.
(28) Johann, C.; Kilz, P. *J. Appl. Polym. Sci.: Appl. Polym. Symp.* **1991**, *48*, 111.
(29) Percec, V.; Ahn, C. H.; Cho, W. D.; Jamieson, A. M.; Kim, J.; Leman, T.; Schmidt, M.; Gerle, M.; Moller, M.; Prokhorova, S. A.; Sheiko, S. S.; Cheng, S . Z. D.; Zhang, A.; Ungar, G.; Yeardley, D. J. P. *J. Am. Chem. Soc.* **1998**, *120*, 8619.
(30) Gerle, M.; Fischer, K.; Roos, S.; Muller, A. H. E.; Schmidt, M.; Sheiko, S. S.; Prokhorova, S.; Moller, M. *Macromolecules* **1999**, *32*, 2629.

MA001248B